International Journal of Heat and Mass Transfer 52 (2009) 3364–3372

Contents lists available at ScienceDirect

International Journal of Heat and Mass Transfer

journal homepage: www.elsevier.com/locate/ijhmt

Effects of jet pattern on two-phase performance of hybrid micro-channel/micro-circular-jet-impingement thermal management scheme

Myung Ki Sung, Issam Mudawar *

Boiling and Two-Phase Flow Laboratory (BTPFL), Purdue University International Electronic Cooling Alliance (PUIECA), Mechanical Engineering Building, 585 Purdue Mall West Lafayette, IN 47907-2088, USA

ARTICLE INFO

Article history:
Received 27 February 2008
Received in revised form 12 June 2008
Available online 26 March 2009

ABSTRACT

This paper explores the two-phase cooling performance of a hybrid cooling scheme in which a linear array of micro-jets deposits liquid gradually along each channel of a micro-channel heat sink. The study also examines the benefits of utilizing differently sized jets along the micro-channel. Three micro-jet patterns, decreasing-jet-size (relative to center of channel), equal-jet-size and increasing-jet-size, were tested using HFE 7100 as working fluid. It is shown feeding subcooled coolant into the micro-channel in a gradual manner greatly reduces vapor growth along the micro-channel. Void fraction increased between jets but decreased sharply beneath each jet, creating a repeated pattern of growth followed by coalesce, and netting only a mild overall increase in void fraction along the flow direction with predominantly liquid flow at outlet. Unlike most flow boiling situations, where pressure drop increases with increasing heat flux, pressure drop in the hybrid configurations actually decreased and reached a minimum just before CHF. This behavior is closely related to the low void fraction and predominantly liquid flow. Pressure drop in the two-phase region is highest for the equal-jet-size pattern, followed by the decreasing-jet-size and increasing-jet-size patterns, respectively. Low void fraction increased the effectiveness of the hybrid cooling schemes in utilizing bulk liquid subcooling and therefore helped achieve high CHF values. The decreasing-jet-size pattern, which had the highest outlet subcooling, achieved the highest CHF. A single correlation was constructed for the three jet patterns, which relates the two-phase heat transfer coefficient to heat flux and wall superheat.

1. Introduction

Micro-channel heat sinks and impinging jets are two effective means for removing highly concentrated heat loads from small surface areas. This is especially the case when the coolant undergoes phase change. The large increase in the slope of the boiling curve following the commencement of boiling offers two key cooling advantages. First, this slope increase means large heat fluxes may be dissipated at relatively low surface temperatures compared to single-phase cooling. Second, relatively large fluctuations in heat flux can be managed with minor changes in surface temperature [1]. Another important advantage of both two-phase micro-channel heat sinks and two-phase impinging jets is higher critical heat flux (CHF) compared to other cooling configurations. This is especially important for the new generation of defense electronics such as laser and microwave directed energy weapons and radars, where heat fluxes are expected to exceed 1000 W/cm^2 [1].

Two-phase micro-channel heat sinks have been studied extensively for implementation in electronics cooling. While earlier work involved mainly single-phase cooling, using water as working fluid [2], recent literature shows increasing interest in capitalizing upon the merits of phase change using mostly dielectric coolants. Key merits of two-phase micro-channel heat sinks are compactness, the ability to achieve very high heat transfer coefficients with minimal coolant inventory, and the ability to achieve better stream-wise temperature uniformity than single-phase heat sinks [3–7]. Bowers and Mudawar [3–5] provided the earliest framework for designing and modeling two-phase micro-channel heat sinks, including the prediction of pressure drop, CHF, and heat diffusion within the metallic heat sink. They were also the first to point out the complexities of two-phase flow in small channels, including appreciable compressibility and flashing effects, as well as the likelihood of two-phase choking. Jiang et al. [6] conducted flow visualization studies of water boiling in triangular micro-cannels. They showed that increasing the heat flux triggers an abrupt change in flow pattern to unstable slug flow. Qu and Mudawar [7] identified two types of flow instability in two-phase micro-channel heat sinks, severe pressure drop oscillation and mild parallel channel instability. The severe pressure drop oscillation causes strong flow pattern fluctuations caused by interaction between the two-phase mixture in the heat sink's micro-channels and the upstream compressible volume in the coolant delivery

* Corresponding author. Tel.: +1 765 494 5705; fax: +1 765 494 0539.
E-mail addresses: mudawar@ecn.purdue.edu, dongqing.li@ualberta.ca (I. Mudawar).

0017-9310/$ - see front matter © 2009 Elsevier Ltd. All rights reserved.
doi:10.1016/j.ijheatmasstransfer.2008.06.046

Nomenclature

A_t	top test surface area of copper heating block ($1.0 \times 2.0\ cm^2$)
C	empirical constant
D_{jet}	micro-jet diameter
$\bar{h}$	mean convective heat transfer coefficient
$\bar{h}_{tp}$	mean two-phase heat transfer coefficient
L	length of unit cell (also length of micro-channel)
L_{jet}	pitch of micro-jet
$L_{jet,i}$	length of micro-channel associated with jet i
$\dot{m}$	mass flow rate of entire cooling module
n	empirical constant
P	pressure
P_W	total electrical power input to cartridge heaters
Q	volumetric flow rate of entire cooling module
q''_{eff}	effective heat flux based on top test surface area of copper block
q''_m	critical heat flux based on top test surface area of copper block
T	temperature
T_{in}	fluid temperature at test module inlet
T_{out}	fluid temperature at test module outlet
$\overline{T}_s$	mean wall temperature
ΔT_{sat}	wall superheat, $\overline{T}_s - T_{sat}$
ΔT_{sub}	subcooling, $T_{sat} - T_{in}$
W	width of unit cell
W_{ch}	width of micro-channel
W_w	half-width of copper wall separating micro-channels
x	Cartesian coordinate
y	Cartesian coordinate

Greek symbols

ρ	density
ϕ	fluid phase (vapor or liquid)

Subscripts

Ch	micro-channel
Cor	correlation
exp	experiment
f	liquid
in	test module inlet
m	maximum (CHF)
out	test module outlet
s	test surface
sat	saturation
sub	subcooling
tp	two-phase

system, and can induce premature CHF. This form of instability could be virtually eliminated by throttling the flow just upstream of the heat sink. The mild parallel channel instability is harder to overcome, despite the upstream throttling. However, it is less taxing on the cooling system and the device being cooled because of relatively mild pressure and temperature fluctuations. Another important drawback of two-phase micro-channel heat sinks is large pressure drop, which is caused by both small hydraulic diameter and large void fraction.

Two-phase jet-impingement cooling has been investigated experimentally. Mudawar and Wadsworth [8] examined the cooling of a $12.7 \times 12.7\ mm^2$ heat source by a confined slot jet using FC-72 as working fluid. Confining the flow helped prevent the separation of the wall jets from the surface by the vapor momentum; this separation can lead to premature CHF. They obtained a comprehensive database including broad variations of jet width, orifice-to-surface distance, jet velocity and subcooling, and developed a CHF correlation for confined jet impingement. Yang et al. [9] conducted experiments with a free circular jet impinging on a rectangular heated surface. They showed a high degree of subcooling greatly suppresses bubble growth by condensation. In most two-phase jet studies, investigators found no obvious influence of jet velocity on the relationship between the heat flux and the wall superheat within the nucleate boiling region [10,11]. Overall, two-phase jet-impingement has the capacity to dissipate very large heat fluxes corresponding to relatively small pressure drops. A key concern, however, is that jets concentrate the cooling within the immediate vicinity of the stagnation zone. Using multiple jets does reduce this concentrated cooling effect, however, multiple jets can obstruct the flow of the spent fluid and induce complex flow instabilities between jets, especially when using a large number of jets to cool a single heat source [1]. Monde et al. [12] investigated the combined influence of multiple jet-impingement on nucleate boiling heat transfer using water and R-113 as working fluids.

Recently, the present authors developed a 'hybrid cooling' concept that capitalizes upon the advantages of both micro-channel flow and jet impingement while avoiding the disadvantages of both. Using this hybrid cooling technology, a single long slot jet [13–15] or a linear array of equally sized circular jets [16] supply coolant into each micro-channel of a multi-channel heat sink to which an electronic device is attached. Within each micro-channel, the flow is divided into two equal and opposite parts, each leading to an outlet plenum. Introducing the coolant gradually into each channel provides a means for controlling surface temperature gradients in a manner not available with conventional micro-channels. Furthermore, controlling the flow of spent fluid within individual micro-channels eliminates the aforementioned instabilities prevalent in conventional multi-jet-impingement modules. This study is an extension of the authors' previous work [17] that explored the benefits of utilizing differently sizes jets along the micro-channel to single-phase cooling performance; the present study concerns two-phase cooling performance.

In the present study, three different jet patterns are examined. Each pattern is defined by jet-size changes symmetrically from the center of the micro-channel towards the outlet plenums. The decreasing-jet-size pattern, equal-jet-size pattern, and increasing-jet-size pattern differ in the manner they modulate the relative contributions of jet impingement and micro-channel flow along the micro-channel. The performances of the three patterns are compared relative to the magnitude of two-phase heat-transfer coefficient, average surface temperature, pressure drop and CHF.

2. Experimental methods

2.1. Test loop

A fluid conditioning system was constructed to deliver HFE 7100 liquid to the test module housing the hybrid cooling hardware at the desired pressure, temperature and flow rate. As illustrated in Fig. 1, the system consists of a primary HFE 7100 loop that contains the test module, and a secondary low temperature refrigeration system. Three needle valves in the primary loop are

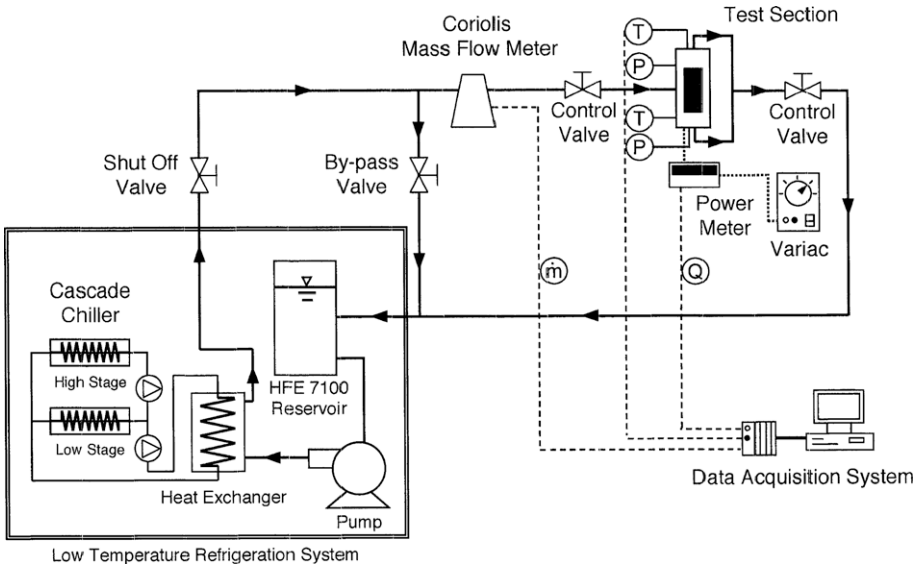

Fig. 1. Schematic of flow loop.

used to control both the flow rate and test module's outlet pressure. The flow rate is measured by a Coriolis flow meter. Heat from the primary coolant is rejected to the refrigeration system via a heat exchanger. Feedback control in the refrigeration system regulates the temperature of the primary coolant to within ±0.5 °C.

2.2. Test module

Fig. 2 illustrates the construction and assembly of the test module. This module consists of a copper heating block, a micro-jet plate, an upper housing, a bottom housing, lower support plates, and sixteen cartridge heaters. The micro-channels are equidistantly formed by cutting five 1-mm wide by 3-mm deep slots within the 10-mm width of the top $10 \times 20\ mm^2$ test surface of the copper heating block. The heating block is stepped to help ensure uniform temperature along the top test surface. The underside of the heating block is bored to accommodate the sixteen cartridge heaters, which supply the heat to the micro-channels. The total electrical power input to the cartridge heaters is measured by a Yokogawa WT210 wattmeter. Both the upper and bottom housings are fabricated from high-temperature G-11 fiberglass plastic. The upper housing includes an inlet plenum that is located above the micro-jet plate. The primary coolant, HFE 7100, is supplied though holes in the micro-jet plate in the form of jets that impinge inside the micro-channels. The flow splits into two equal and opposite parts in the micro-channels; each is expelled into one of two plenums in the bottom housing. Four type-T thermocouples are inserted below the micro-channel's bottom wall. An absolute pressure transducer and a type-T thermocouple are connected to the inlet plenum in the upper housing. Another absolute pressure transducer and a second thermocouple are each connected to one of the outlet plenums in the bottom housings. Four stainless steel

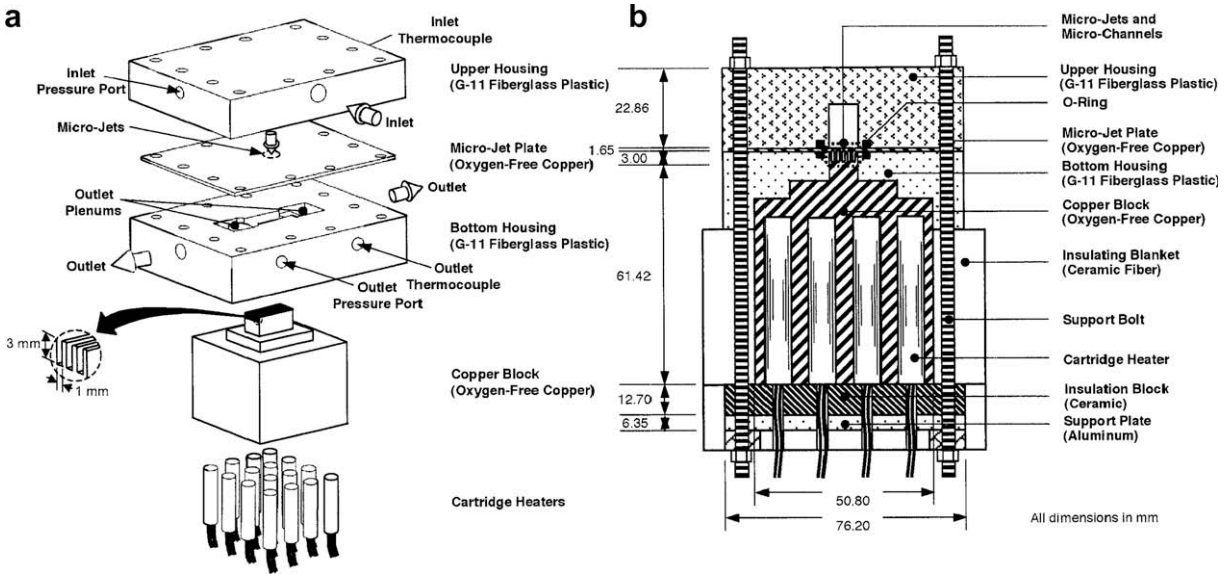

Fig. 2. (a) Test module construction. (b) Cross-section of test module assembly.

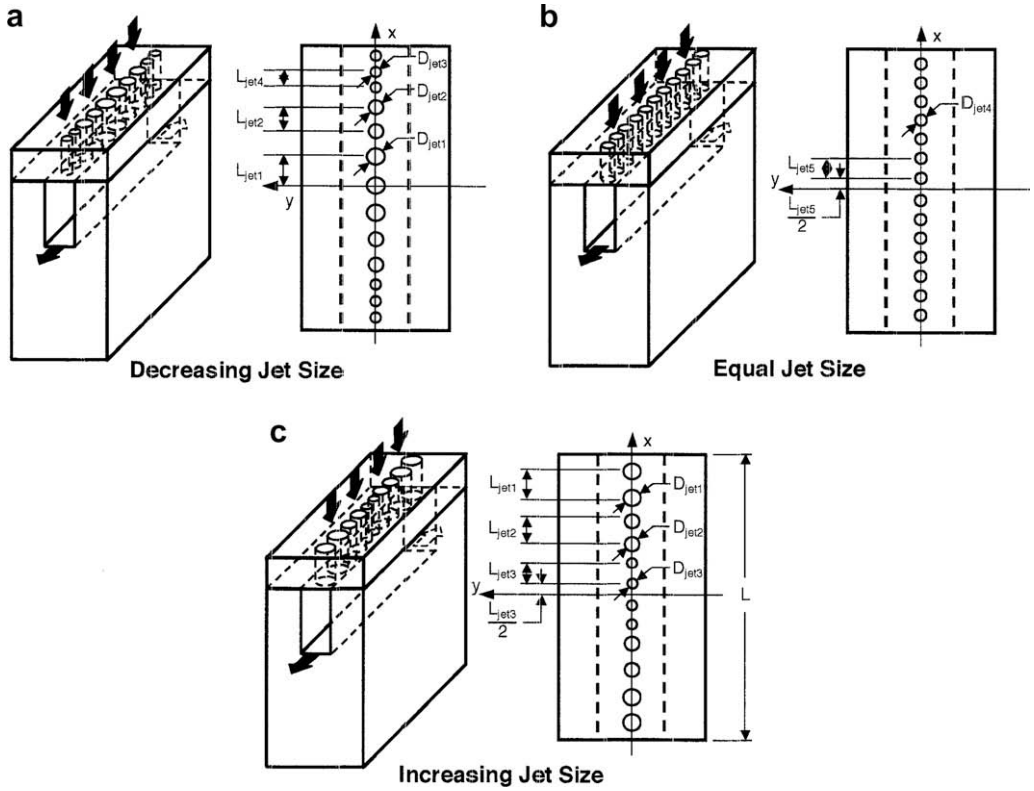

Fig. 3. Schematic of unit cell illustrating patterns of (a) decreasing jet size, (b) equal jet size, and (c) increasing jet size.

pins traverse the top housing, jet plate and copper block to ensure accurate placement of the micro-jets relative to the micro-channels.

2.3. Jet patterns

Three different micro-jet patterns are examined; each pattern is formed in a separate micro-jet plate. A unit cell consisting of a single micro-channel and portion of the micro-jet plate facing the same micro-channel is illustrated in Fig. 3. The figure also shows the different geometrical parameters of the unit cell. The first micro-plate has jets decreasing in size along each side of the micro-channel. The second jet plate has equally-sized jets. Jets in the third jet plate increase in size from the center of the micro-channel.

The three micro-jet plates are fabricated from oxygen-free copper. In each plate, five parallel arrays of circular holes are drilled within the 1-cm width facing the five micro-channels. The total cross-sectional area of the holes is equal for all three jet plates. Fig. 4 shows photos of the three micro-jet plates. Detailed dimensions of the micro-jet plates are given in Table 1.

2.4. Operating procedure and measurements

Boiling curves were measured for each of the three jet patterns subject to variations in coolant flow rate and inlet temperature. Once the required operating conditions were achieved, electric power was supplied to the test module's cartridge heaters in small increments up to CHF. Key parameters were measured after steady state was achieved following each power increment. These include module inlet pressure, P_{in}, outlet pressure, P_{out}, inlet temperature, T_{in}, outlet temperature, T_{out}, heating block thermocouple temperatures, and heater power input, P_W.

The total volumetric flow rate was determined from the measured mass flow rate, $\dot{m}$, and coolant density, ρ_f,

$$Q = \frac{\dot{m}}{\rho_f}. \tag{1}$$

The effective heat flux, q''_{eff}, from the top test surface of the copper heating block was determined by dividing the total electrical power input, P_W, by the test surface area, $A_t = 10 \times 20\ \text{mm}^2$.

$$q''_{eff} = \frac{P_W}{A_t}. \tag{2}$$

The heat transfer coefficient was calculated from

$$\bar{h} = \frac{q''_{reff}}{(\overline{T}_s - T_{in})} \tag{3}$$

where $\overline{T}_s$ is the mean temperature of the test surface.

Special attention was given to minimizing heat loss from the copper block. A 3-D numerical model of the entire test module yielded a heat loss to the ambient of less than 4% of the electrical power input during the two-phase region. The heat fluxes reported in the present paper are therefore based on the measured electrical power input.

Measurement uncertainties associated with the pressure transducers, flow meter, wattmeter, and thermocouples are 0.5%, 0.1%, 0.5%, and 0.3° C, respectively. Table 2 summarizes the operating conditions of the study.

3. Results and discussion

3.1. Boiling curve trends

Since high-flux electronic and power devices for which the present cooling scheme is intended undergo power fluctuations during normal operation, it is important to determine the temperature response of the device to these power fluctuations. Of special importance is the ability to produce the same temperature for a given heat flux value regardless how this heat flux is reached. Nucle-

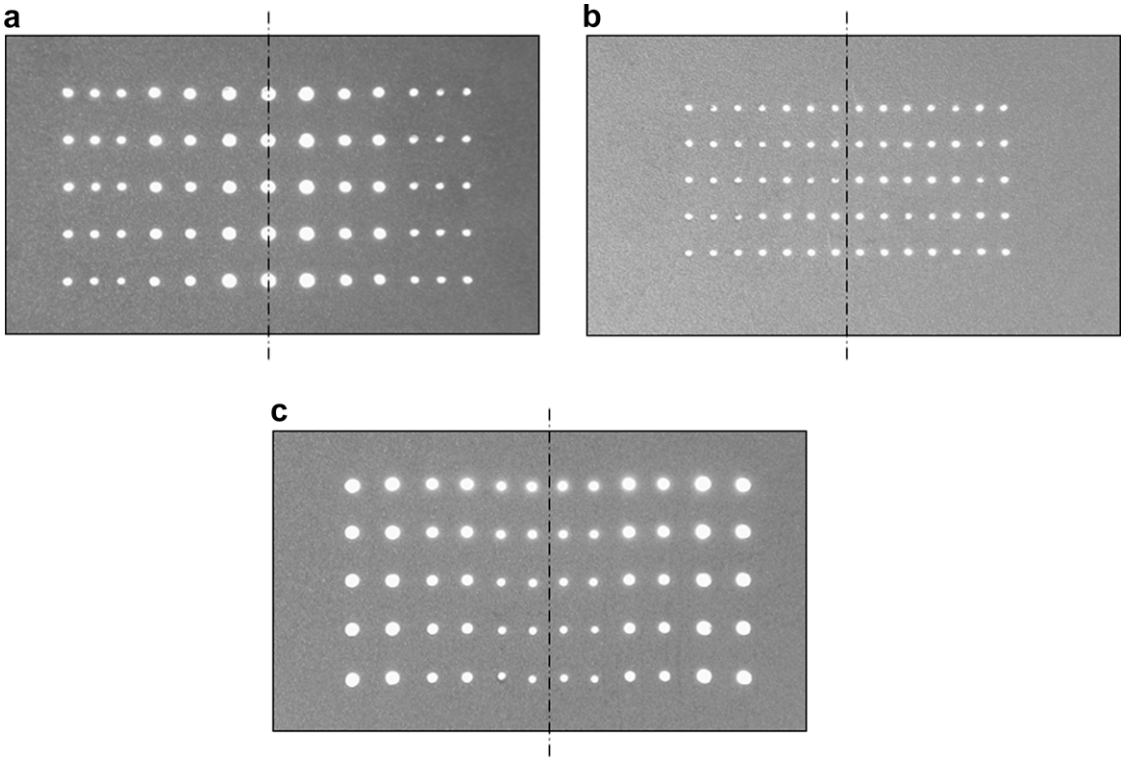

Fig. 4. Photos of jet plates with patterns of (a) decreasing jet size, (b) equal jet size, and (c) increasing jet size.

Table 1
Dimensions of unit cell.

L (mm)	L_{jet1} (mm)	L_{jet2} (mm)	L_{jet3} (mm)	L_{jet4} (mm)	L_{jet5} (mm)	W (mm)
20.00	1.84	1.62	1.44	1.23	1.43	1.83
W_{ch} (mm)	W_w (mm)	D_{jet1} (mm)	D_{jet2} (mm)	D_{jet3} (mm)	D_{jet4} (mm)	
1.00	0.42	0.60	0.45	0.30	0.42	

Table 2
Experimental operating conditions.

Working fluid	Inlet temperature T_{in} (°C)	Inlet flow rate $\dot{m}$(g/s)	Effective heat flux q''_{eff}(W/cm^2)
HFE 7100	−40 to 20	11.1–55.9	16.1–505

ate boiling performance can manifest significant hysteresis depending on whether a particular operating condition is achieved by increasing or decreasing the heat flux. Hysteresis is encountered both at the onset of boiling and throughout the nucleate boiling region. Virtually all dielectric fluids used in electronics cooling are prone to incipient boiling hysteresis. Because of the low contact angle of these coolants, liquid can easily flood cavities, depriving potential nucleation sites from the vapor embryos necessary to initiate and sustain the boiling process [1]. When increasing the heat flux from a non-boiling state, appreciable wall superheat – overshoot – is required to initiate the boiling process. Once boiling is initiated, the ensuing large increase in the heat transfer coefficient causes a sudden decrease in the wall temperature. The large incipient wall superheat and ensuing temperature drop are highly troublesome in electronics cooling because of the potential for thermal shock to the device. Increasing the heat flux beyond the incipience point follows a fairly predictable relationship between the heat flux and wall temperature. Similar behavior is achieved when decreasing the heat flux. However, the transition from nucleate boiling to single-phase cooling occurs without the aforementioned incipience overshoot, hence the term hysteresis. Another form of hysteresis is manifest in differences in the wall temperature in the nucleate boiling region when increasing versus decreasing the heat flux.

Fig. 5 shows boiling curves that were measured by increasing and decreasing the heat flux for the decreasing-jet-size pattern at $Q = 2.33 \times 10^{-5}$ m^3/s and $T_{in} = 0°$ C. Heat flux in these tests was increased in small increments up to CHF and then decreased again in small increments. The mean surface temperature, $\overline{T}_s$, in Fig. 5 was determined as follows. First, local surface temperatures were calculated by correcting the thermocouple temperatures for one-dimensional heat conduction between the thermocouple location and the test surface immediately above. These temperatures were then area-averaged to determine $\overline{T}_s$. The inlet temperature was measured by the thermocouple located in the inlet plenum. Fig. 5 shows the two boiling curves are identically matched, proving the hybrid cooling scheme precludes both forms of hysteresis.

Fig. 6 shows the effects of flow rate on the boiling curve for the three jet patterns. For each pattern, increasing the flow rate augments single-phase heat transfer considerably and delays the onset of nucleate boiling (ONB) to a higher heat flux. Boiling curves tend to converge in the nucleate boiling region, which is consistent with findings from previous jet impingement studies [8,11]. Increasing flow rate also enhances CHF appreciably. Notice that not all boiling curves culminate in CHF. High flow rate tests produced very high temperatures in the heating block and had to be terminated before CHF to prevent any permanent damage to the test module.

Fig. 7 shows the effects of subcooling on the boiling curve for the three jet patterns at $Q = 7.66 \times 10^{-6}$ m^3/s. For each pattern, increasing the subcooling delayed the onset of boiling and CHF to

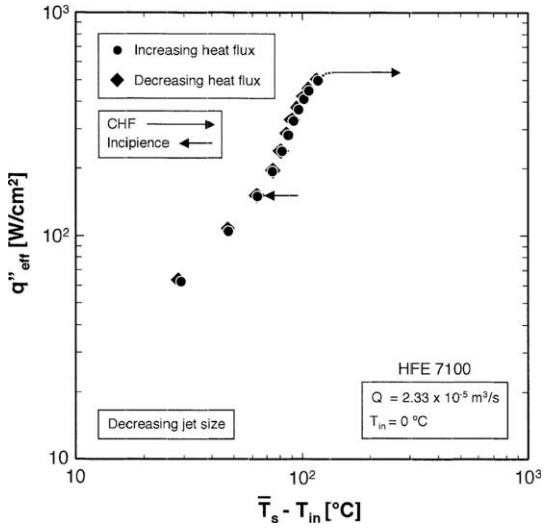

Fig. 5. Boiling curves corresponding to increasing and decreasing heat flux for decreasing-jet-size pattern.

both higher heat fluxes and higher surface temperatures. Overall, Fig. 7 shows the decreasing-size-jet pattern achieves the highest CHF at a given level of subcooling followed, respectively, by the equal-jet-size and increasing-jet-size patterns. Those differences in boiling behavior among the different jet patterns are closely related to the fact that the present hybrid cooling configurations are associated with very mild void fractions (this issue will be discussed later), where bulk liquid flow plays a major role even in the nucleate boiling region. In a previous study by the authors on differences in single-phase performance among the three jet patterns [17], numerical simulations showed the decreasing-jet-size pattern yields the lowest surface temperature (i.e., highest heat transfer coefficient), followed by the equal-jet-size and increasing-jet-size patterns, respectively. This also implies the decreasing-jet-size pattern delays the onset of boiling to a higher flux and decreases void fraction compared to the other two patterns. With a lower void fraction, the decreasing-jet-size pattern provides greater access of subcooled bulk liquid to the wall, resulting in the highest CHF for this pattern. The single-phase numerical simulations also showed the equal-jet-size pattern provides the greatest surface temperature uniformity, while the fluid flow with the increasing-jet-size pattern is complicated by blockage from the large jets located near the channel outlet.

3.2. Pressure drop

Fig. 8(a) shows the variation of pressure drop with heat flux for the decreasing-jet-size pattern at $Q = 7.45 \times 10^{-6}$ m^3/s and four subcoolings. For the single-phase region, pressure drop decreases with increasing temperature because of reduced viscosity. Fig. 8(a) shows pressure drop decreases with increasing heat flux for each inlet temperature because of this viscosity effect. Interestingly, this trend continues into the two-phase region, with the minimum pressure drop encountered just before CHF. This is contrary to trends found in most flow boiling situations, where pressure drop increases appreciably in the two-phase region. This unusual trend may be explained by the fundamentally different nucleate boiling pattern encountered in the hybrid cooling configuration compared to conventional micro-channel two-phase flow. As illustrated in Fig. 9(a), void fraction in conventional micro-channel flow increases monotonically along the micro-channel, increasing both the frictional and accelerational components of pressure drop. In the hybrid cooling configuration, Fig. 9(b), void fraction increases gradually between jets before being greatly reduced by condensation beneath the jets. This results is a repeated pattern

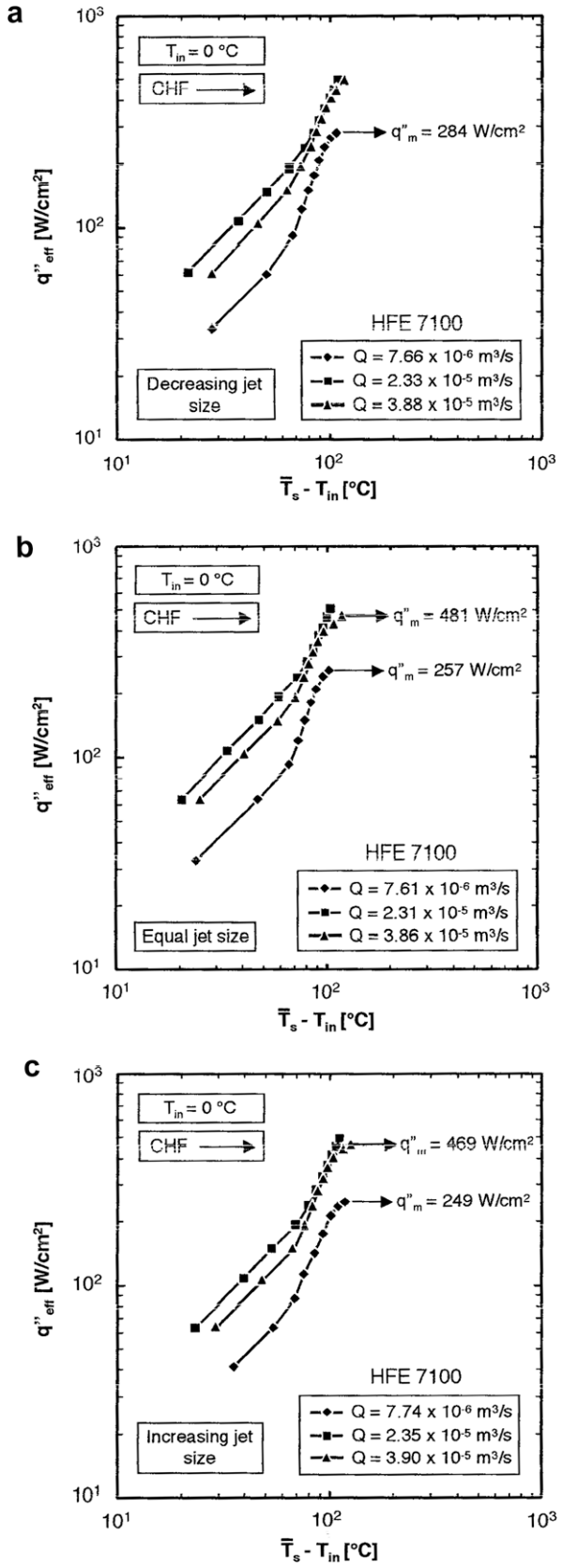

Fig. 6. Effects of flow rate on boiling curve for patterns of (a) decreasing jet size, (b) equal jet size, and (c) increasing jet size.

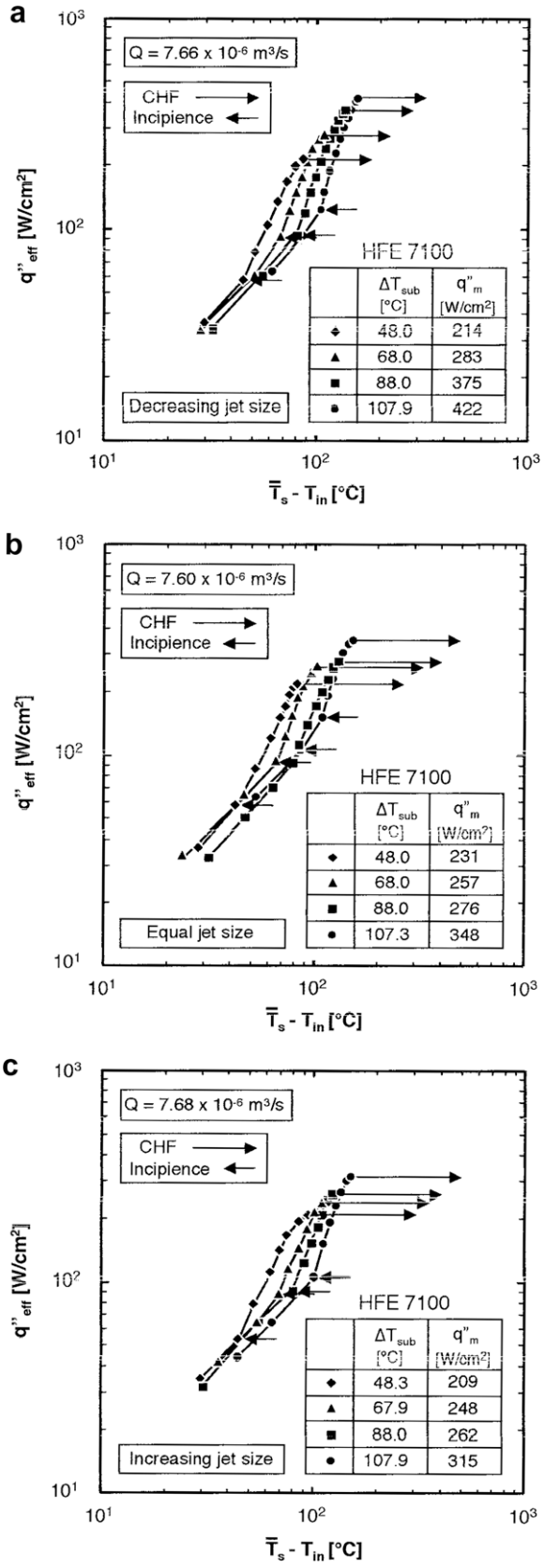

Fig. 7. Effects of subcooling on boiling curve for patterns of (a) decreasing jet size, (b) equal jet size, and (c) increasing jet size.

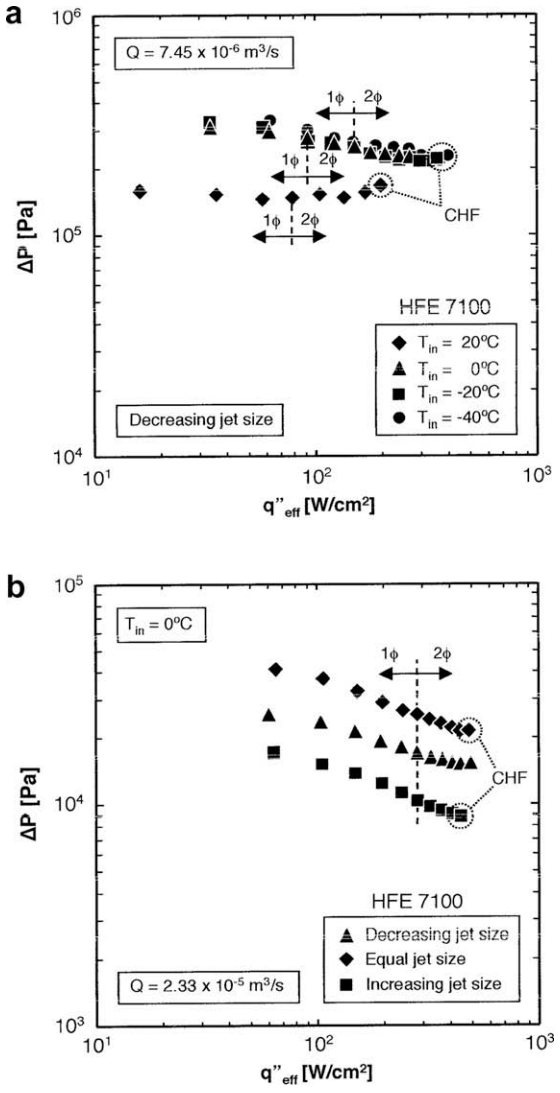

Fig. 8. (a) Variation of pressure drop with heat flux for different inlet temperatures for decreasing-jet-size pattern. (b) Variation of pressure drop with heat flux for different jet patterns.

of void fraction growth and collapse along the micro-channel, and a mild overall increase in void fraction along both sides of the micro-channel. Small void fraction results in both small pressure drop and pressure drop characteristics that are dominated by liquid friction.

Fig. 8(b) shows the variation of pressure drop with heat flux for the three jet patterns at $Q = 2.33 \times 10^{-5}$ m^3/s and $T_{in} = 0$ °C. Data for all patterns follow a trend of decreasing pressure drop with increasing heat flux because of the reduced liquid viscosity. This trend also persists in the two-phase region because of the mild overall increase in void fraction along the micro-channel. Feeding subcooled liquid from jets gradually along the micro-channel appears to help maintain a predominantly liquid state at the micro-channel outlet with a relatively small mass of vapor confined to the micro-channel walls. CHF is consistent with the mechanism of Departure from Nucleate Boiling (DNB) associated with highly subcooled flow boiling, high mass velocities, and small length-to-diameter ratios [18]. Fig. 8(b) shows pressure drop is highest for the equal-jet-size pattern followed, respectively, by the decreasing-jet-size and increasing-jet-size patterns.

3.3. Two-phase heat transfer

Fig. 10 shows the variation of outlet fluid temperature with heat flux for the three jet patterns at $Q = 2.33 \times 10^{-5}$ m^3/s and $T_{in} = 0°$ C.

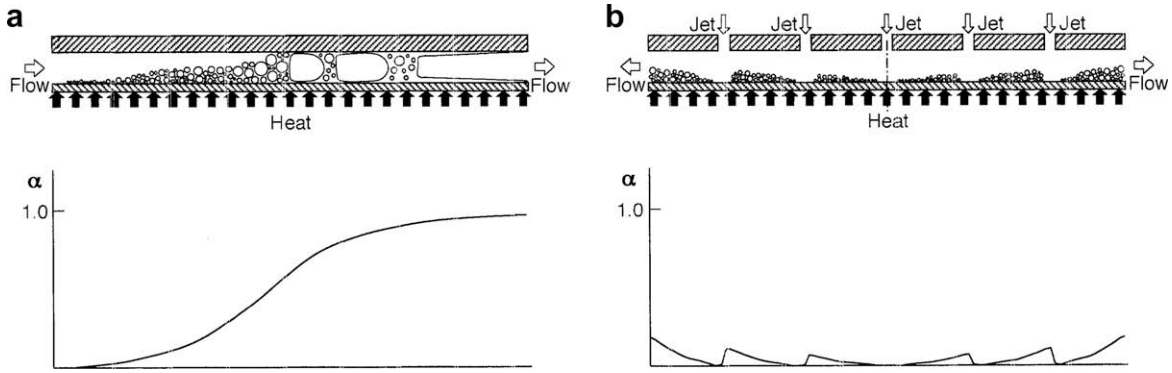

Fig. 9. Schematic representation of vapor growth and variation of void fraction along micro-channel for (a) conventional micro-channel and (b) hybrid cooling configuration.

These trends are consistent with the earlier discussion concerning outlet surface and fluid temperatures. Fig. 10 shows the decreasing-jet-size patterns produced the lowest temperatures followed, respectively, by the equal-jet-size and increasing-jet-size patterns.

Fig. 11(a) shows the variation of the area-averaged surface temperature with heat flux at $Q = 7.50 \pm 0.1 \times 10^{-6}$ m^3/s and $T_{in} = 40°$ C. For the high flux data preceding CHF, lowest surface temperatures are achieved with the decreasing-jet-size pattern followed by the equal-jet-size and increasing jet-size patterns, respectively, in accordance with the trend captured in Fig. 10 for outlet fluid temperature.

Fig. 11(b) shows the heat transfer coefficient in the two-phase region preceding CHF is also highest for the decreasing-jet-size pattern followed by the equal-jet-size and increasing-jet-size patterns, respectively. This trend in consistent with the above-mentioned (1) strong influence of single-phase liquid flow, and (2) the trend of lowest wall and fluid outlet temperatures for the decreasing-jet-size pattern. Fig. 11(b) shows the decreasing-jet-size pattern also produces the highest CHF because of low void fraction and better access of subcooled bulk liquid to the wall.

Nonetheless, Fig. 11(b) shows heat transfer coefficient variations among jet patterns are relatively small; those variations are quite significant for single-phase flow [17]. The present results point to the possibility of developing a universal two-phase heat transfer coefficient correlation applicable to all three patterns.

In previous studies by the present authors, nucleate boiling data for the hybrid cooling scheme using both micro-slot jets [15] and equally-sized micro-circular jets [16], were correlated using the following relations between heat flux and wall superheat.

$$q''_{reff} = C\Delta T^{n}_{sat} \tag{4}$$

$$\text{and } q''_{reff} = \bar{h}_{tp}(\overline{T}_s - T_{in}) = \bar{h}_{tp}(\Delta T_{sat} + \Delta T_{sub}). \tag{5}$$

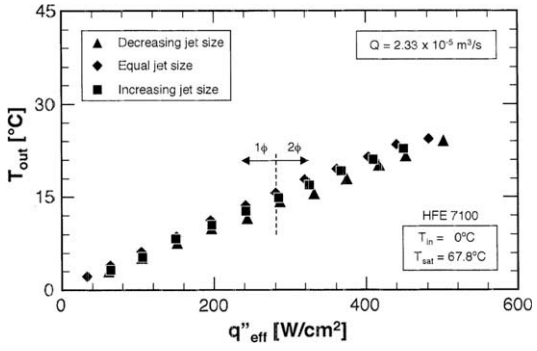

Fig. 10. Variation of micro-channel outlet temperature with heat flux for different jet patterns at $Q = 2.33 \times 10^{-5}$ m^3/s and $T_{in} = 0$ °C.

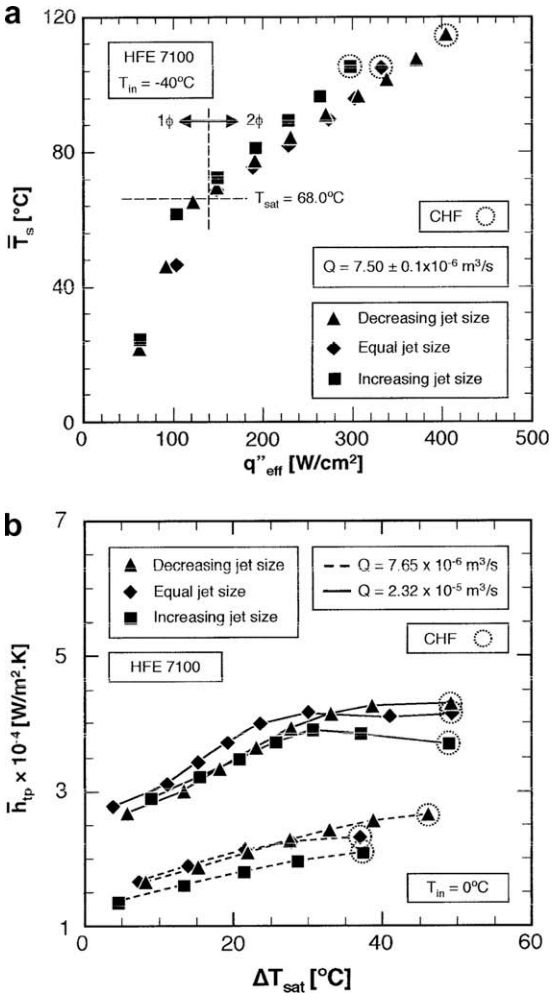

Fig. 11. (a) Variation of surface temperature with heat flux for three jet patterns at $Q = 3.87 \times 10^{-5}$ m^3/s and $T_{in} = 40°$ C. (b) Variation of two-phase heat transfer coefficient with wall superheat for three jet patterns at two flow rates and $T_{in} = 0$ °C.

Combining these relations yields a general relationship for the two-phase heat transfer coefficient.

$$\bar{h}_{tp} = \frac{q''_{ref}}{\left(\frac{q''_{eff}}{C}\right)^{1/n} + \Delta T_{sub}} \tag{6}$$

The empirical constants n and C in the above equation were obtained by a least-squares' fit to the entire nucleate boiling database for all three jet patterns, resulting in the correlation

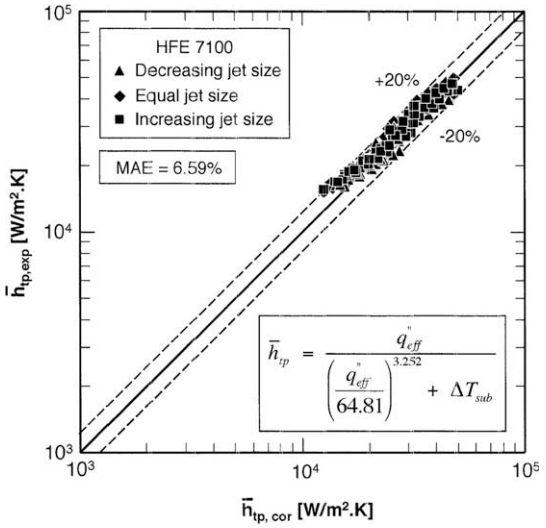

Fig. 12. Comparison of predictions of two-phase heat transfer coefficient correlation with HFE 7100 data.

$$\bar{h}_{tp} = \frac{q''_{eff}}{\left(\frac{q''_{eff}}{64.81}\right)^{1/3.252} + \Delta T_{sub}} \tag{7}$$

Fig. 12 shows the above correlation is equally successful at predicting 155 nucleate boiling data points for the three jet patterns, evidenced by a mean absolute error of only 6.59%.

4. Conclusions

This study examined a two-phase hybrid cooling scheme that combines the cooling benefits of micro-channel flow and micro-jet impingement. Three micro-jet patterns were examined, decreasing-jet-size, equal-jet-size and increasing-jet-size. The performance of each pattern was examined experimentally using HFE 7100 as working fluid. Key findings from the study are as follows:

1. The hybrid cooling configuration provides a two-phase cooling performance that is free from the incipient boiling overshoot and temperature drop, which are prevalent in many boiling situations involving low contact angle liquids. Furthermore, virtually identical boiling curves are achieved by increasing and decreasing heat flux, proving this configuration is void of nucleate boiling hysteresis. These attributes render the hybrid cooling scheme highly effective for electronics cooling applications.
2. Feeding subcooled coolant into the micro-channel in a gradual manner greatly reduces vapor growth along the micro-channel. Void fraction increases between jets but decreases sharply beneath the jets. This creates an unusual pattern of void fraction growth followed by coalesce, and a relatively mild overall increase along the flow direction with predominantly liquid flow at outlet.
3. Pressure drop in the single-phase region decreases with increasing heat flux because of decreasing liquid viscosity. However, unlike most flow boiling situations, where pressure drop begins increasing in the nucleate boiling region, pressure drop in the hybrid configuration continues decreasing and reaches a minimum just before CHF. This behavior is closely related to the low void fraction and predominantly liquid flow. Pressure drop in the two-phase region is highest for the equal-jet-size pattern, followed by the decreasing-jet-size and increasing-jet-size patterns, respectively.
4. Because of the mild void fraction, the hybrid cooling configuration is highly effective at utilizing the bulk liquid subcooling to achieve high CHF values. It is postulated CHF mechanism is similar to that of Departure from Nucleate Boiling (DNB) encountered in channel flow with high flow rates, high subcoolings and small length-to-diameter ratios. Highest CHF values are achieved with the decreasing-jet-size pattern because this pattern yields the highest outlet subcooling.
5. A single correlation is constructed for the three jet patterns, which relates the two-phase heat transfer coefficient to heat flux and wall superheat. The correlation predicts the two-phase HFE 7100 data with a mean absolute error of 6.59%.

Acknowledgement

The authors are grateful for the financial support of the Office of Naval Research (ONR).

References

[1] I. Mudawar, Assessment of high-heat-flux thermal management schemes, IEEE Trans. – Compon. Packaging Tech. 24 (2001) 122–141.
[2] D.B. Tuckerman, R.F.W. Pease, High-performance heat sinking for VLSI, IEEE Electron. Dev. Lett. EDL-2 (1981) 126–129.
[3] M.B. Bowers, I. Mudawar, High flux boiling in low flow rate, low pressure drop mini-channel and micro-channel heat sinks, Int. J. Heat Mass Transfer 37 (1994) 321–332.
[4] M.B. Bowers, I. Mudawar, Two-phase electronic cooling using mini-channel and micro-channel heat sinks – Part 1. Design criteria and heat diffusion constraints, ASME J. Electronic Packaging 116 (1994) 290–297.
[5] M.B. Bowers, I. Mudawar, Two-phase electronic cooling using mini-channel and micro-channel heat sinks – Part 2. Flow rate and pressure drop constraints, ASME J. Electron. Packaging 116 (1994) 298–305.
[6] L. Jiang, M. Wong, Y. Zohar, Forced convection boiling in a microchannel heat sink, J. Microelectromech. Syst. 10 (2001) 80–87.
[7] W. Qu, I. Mudawar, Measurement and prediction of pressure drop in two-phase micro-channel heat sinks, Int. J. Heat Mass Transfer 46 (2003) 2737–2753.
[8] I. Mudawar, D.C. Wadsworth, Critical heat flux from a simulated electronic chip to a confined rectangular impinging jet of dielectric liquid, Int. J. Heat Mass Transfer 34 (1991) 1465–1480.
[9] C. Yang, A.A.O. Tay, H. Xue, An experimental study of liquid jet impingement cooling of electronic components with and without boiling, in: Proceedings of the Advances in Electronics Material and Packaging, IEEE, Nov. 19–22, Jeju Island, Korea, 2001, pp. 369–375.
[10] Y. Katto, M. Kunihiro, Study of the mechanism of burn-out in boiling system of high burn-out heat flux, Bull. JSME 16 (1973) 1357–1366.
[11] D.H. Wolf, F.P. Incropera, R. Viskanta, Local jet impingement boiling heat transfer, Int. J. Heat Mass Transfer 39 (1996) 1395–1406.
[12] M. Monde, H. Kusuda, H. Uehara, Burnout heat flux in saturated forced convection boiling with two or more impinging jets, Heat Transfer – Japanese Res. 9 (1980) 18–31.
[13] M.K. Sung, I. Mudawar, Experimental and numerical investigation of single-phase heat transfer using a hybrid jet impingement/micro-channel cooling scheme, Int. J. Heat Mass Transfer 49 (2006) 682–694.
[14] M.K. Sung, I. Mudawar, Correlation of critical heat flux in hybrid jet impingement/micro-channel cooling scheme, Int. J. Heat Mass Transfer 49 (2006) 2663–2672.
[15] M.K. Sung, I. Mudawar, Single-phase and two-phase cooling using hybrid micro-channel/slot-jet-module, Int. J. Heat Mass Transfer 51 (2008) 3825–3839.
[16] M.K. Sung, I. Mudawar, Single-phase and two-phase heat transfer characteristics of low temperature hybrid micro-channel/micro-jet-impingement cooling, Int. J. Heat Mass Transfer 51 (2008) 3882–3895.
[17] M.K. Sung, I. Mudawar, Effects of jet pattern on single-phase cooling performance of hybrid micro-channel/micro-circular-jet-impingement thermal management scheme, Int. J. Heat Mass Transfer 51 (2008) 4614–4627.
[18] I. Mudawar, M.B. Bowers, Ultra-high critical heat flux (CHF) for subcooled water flow boiling-I: CHF data and parametric effects for small diameter tubes, Int. J. Heat Mass Transfer 42 (1999) 1405–1428.